

Assessing the Slow Magnetic Relaxation Behavior of $\text{Ln}^{\text{III}}_4\text{Mn}^{\text{III}}_6$ Metallocrowns

Curtis M. Zaleski,[§] Jeff W. Kampf,[‡] Talal Mallah,^{*||} Martin L. Kirk,^{*†} and Vincent L. Pecoraro^{*‡}

Department of Chemistry, University of Michigan, Ann Arbor, Michigan 48109-1055,

Department of Chemistry, The University of New Mexico, Albuquerque, New Mexico 87131-0001,

Department of Chemistry, Shippensburg University, Shippensburg, Pennsylvania 17257-2200, and

ICMMO-Equipe Chimie Inorganique UMR CNRS 8182, Univ Paris Sud, 91405 Orsay, France

Received November 14, 2006

A $\text{Dy}^{\text{III}}_4\text{Mn}^{\text{III}}_6$ complex with a metallocrown (MC)-like topology possesses frequency-dependent magnetic behavior, indicating possible single-molecule magnet behavior.

While the synthesis of large lanthanide complexes has recently been of great interest,¹ there remains a paucity of reported large lanthanide (Ln)–transition metal (TM) complexes [i.e., complexes possessing more than five metal centers]. Past research on Ln–TM complexes has primarily focused on small complexes, particularly $\text{Gd}^{\text{III}}\text{–Cu}^{\text{II}}$ systems, with an effort to understand the magnetic exchange between the metal centers.² In addition, several large complexes have also been synthesized with Ln^{III} and Cu^{II} .³ However, very few large $\text{Ln}^{\text{III}}\text{–TM}$ complexes have been realized with other transition metals, although complexes containing Ln ions have shown interesting applications as magnetic resonance imaging contrast agents,⁴ luminescence sensors,⁵ and magnetic particles.⁶ Recently, smaller complexes of Ln^{III} and TM ions have shown single-molecule magnet (SMM) behavior.⁷ Smaller complexes such as $\text{Dy}^{\text{III}}_2\text{Cu}^{\text{II}}_2$ and $\text{Tb}^{\text{III}}_2\text{Cu}^{\text{II}}_2$ were the first to exhibit the phenomenon;^{7a} however, complexes such as $\text{Dy}^{\text{III}}_6\text{Mn}^{\text{III}}_4\text{Mn}^{\text{IV}}_2$,^{7b} $\text{Dy}^{\text{III}}_4\text{Mn}^{\text{III}}_{11}$,^{7c} and $\text{Dy}^{\text{III}}_3\text{Cu}^{\text{II}}_6$ ^{7d}

have extended the SMM phenomenon to larger $\text{Ln}^{\text{III}}\text{–TM}$ complexes. Herein we report a novel $\text{Ln}^{\text{III}}_4\text{Mn}^{\text{III}}_6$ complex that possesses interesting magnetic properties.

Complex **1** [$\text{Ho}^{\text{III}}_4\text{Mn}^{\text{III}}_6(\text{H}_2\text{shi})_2(\text{shi})_6(\text{sal})_2(\text{O}_2\text{CCH}_3)_4(\text{OH})_2(\text{CH}_3\text{OH})_8$] $\cdot 4\text{CH}_3\text{OH}$, where H_3shi is salicylhydroxamic acid and H_2sal is salicylic acid, can be prepared by slowly evaporating the filtrate methanol solvent from the isolation of $\text{Ho}^{\text{III}}_6\text{Mn}^{\text{III}}_4\text{Mn}^{\text{IV}}_2(\text{H}_2\text{shi})_4(\text{Hshi})_2(\text{shi})_{10}(\text{CH}_3\text{OH})_{10}(\text{H}_2\text{O})_2$.² [The synthesis of the analogous Dy^{III} **2** has been reported.^{7b}] After 3 weeks, X-ray quality brown-black needle crystals were obtained and washed with cold methanol. [A synthetic scheme is provide in the Supporting Information.] During this period, some of the original salicylhydroxamic acid was hydrolyzed to the salicylate found in **1**, giving a 10% yield based on the original amount of $\text{Ho}(\text{NO}_3)_3\cdot 5\text{H}_2\text{O}$ used in the synthesis of the parent $\text{Ho}^{\text{III}}_6\text{Mn}^{\text{III}}_4\text{Mn}^{\text{IV}}_2$.

Complex **1** consists of two crystallographically unique Ho^{III} ions and three unique Mn^{III} ions (Figures 1 and S1).⁸ The analogous Dy^{III} complex, **3**, has also been crystallized.⁸ The structure of **1** is best described as a 22-MC-8^{9,10} which

* To whom correspondence should be addressed. E-mail: mallah@icmo.u-psud.fr (T.M.); mlk@unm.edu (M.L.K.); vlpec@umich.edu (V.L.P.).

[‡] University of Michigan.

[†] The University of New Mexico.

[§] Shippensburg University.

^{||} Univ Paris Sud.

- (1) (a) Xu, J.; Raymond, K. N. *Angew. Chem., Int. Ed.* **2000**, *39*, 2745. (b) Kajiwarra, T.; Wu, H.; Ito, T.; Iki, N.; Miyano, S. *Angew. Chem., Int. Ed.* **2004**, *43*, 1832.
- (2) Andruh, M.; Ramade, I.; Codjovi, E.; Guillou, O.; Kahn, O.; Trombe, J. C. *J. Am. Chem. Soc.* **1993**, *115*, 1822.
- (3) (a) Zhang, J. J.; Sheng, T.-L.; Xia, S.-Q.; Leibeling, G.; Meyer, F.; Hu, S.-M.; Fu, R.-B.; Xiang, S.-C.; Wu, X.-T. *Inorg. Chem.* **2004**, *43*, 5472. (b) He, F.; Tong, M.-L.; Chen, X.-M. *Inorg. Chem.* **2005**, *44*, 8285.
- (4) Thompson, M. K.; Botta, M.; Nicolle, G.; Helm, L.; Aime, S.; Merbach, A. E.; Raymond, K. N. *J. Am. Chem. Soc.* **2003**, *125*, 14274.
- (5) Fatin-Rouge, N.; Toth, E.; Perret, D.; Backer, R. H.; Merbach, A. E.; Bunzli, J.-C. G. *J. Am. Chem. Soc.* **2000**, *122*, 10810.
- (6) Regulacio, M. D.; Bussmann, K.; Lewis, B.; Stoll, S. L. *J. Am. Chem. Soc.* **2006**, *128*, 11173.

- (7) (a) Osa, S.; Kido, T.; Matsumoto, N.; Re, N.; Pochaba, A.; Mrozinski, J. J. *Am. Chem. Soc.* **2003**, *125*, 420. (b) Zaleski, C. M.; Depperman, E. C.; Kampf, J. W.; Kirk, M. L.; Pecoraro, V. L. *Angew. Chem., Int. Ed.* **2004**, *43*, 3912. (c) Mishra, A.; Wernsdorfer, W.; Abboud, K. A.; Christou, G. *J. Am. Chem. Soc.* **2004**, *126*, 15648. (d) Aronica, C.; Pilet, G.; Chastanet, G.; Wernsdorfer, W.; Jocquot, J.-F.; Luneau, D. *Angew. Chem., Int. Ed.* **2006**, *45*, 4659.
- (8) Crystals of **1** have been structurally characterized with the formula $\text{Ho}_4\text{Mn}_6\text{C}_9\text{H}_{112}\text{N}_8\text{O}_{54}$. Analytical data for **1** (fw = 3171.25): Found C, 34.25; H, 3.39; N, 3.96; Requires C 34.46; H 3.56; N 3.53. Crystal data for **1**: $M_r = 3171.25$, monoclinic, space group $P2(1)/c$, $a = 14.0149(19)$ Å, $b = 14.421(2)$ Å, $c = 28.304(4)$ Å, $\alpha = 90^\circ$, $\beta = 92.402(6)^\circ$, $\gamma = 90^\circ$, $V = 5715.5(13)$ Å³, $Z = 2$; $d_{\text{calcd}} = 1.843$ mg/m³; $2.91^\circ < \theta < 28.38^\circ$; crystal dimensions (mm³), $0.68 \times 0.06 \times 0.06$; $\mu = 3.492$ mm⁻¹; $T = 113(2)$ K; 14 251 used of 58 744 reflections collected. 14 251 reflections and 792 parameters were used for the full-matrix, least-squares refinement of F^2 , $R_1 = 0.0390$ [$I > 2\sigma(I)$], $R_1 = 0.0609$ (all data); $wR_2 = 0.0795$ [$I > 2\sigma(I)$], $wR_2 = 0.0862$ (all data). All non-hydrogen atoms were refined anisotropically with the hydrogen atoms placed in idealized positions. Further details are given in the Supporting Information for **1** and **3**.
- (9) Lah, M. S.; Pecoraro, V. L. *J. Am. Chem. Soc.* **1989**, *111*, 7258.
- (10) Pecoraro, V. L.; Stemmer, A. J.; Gibney, B. R.; Bodwin, J. J.; Wang, H.; Kampf, J. W.; Barwinski, A. In *Progress in Inorganic Chemistry*; Karlin, K. D., Ed.; John Wiley and Sons, Inc.: New York, 1997; Vol. 45, p 83.

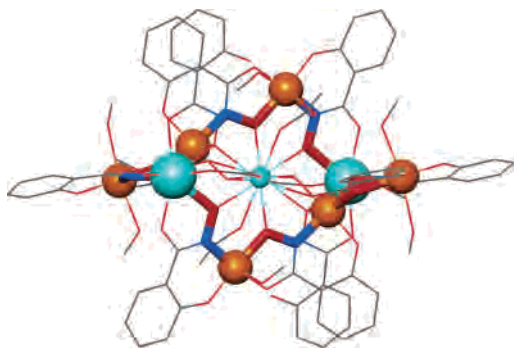


Figure 1. X-ray crystal structure of **1** along the 2-fold axis. The Ho^{III} ions encapsulated by the MC ring are nearly eclipsed. Color scheme: orange spheres, Mn^{III}; aqua spheres, Ho^{III}; red tubes, oxygen; blue tubes, nitrogen. Lattice solvent molecules and hydrogen atoms have been removed for clarity.

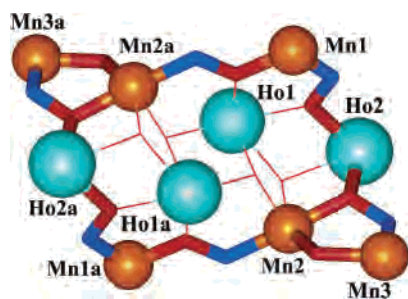


Figure 2. Highlight of the 22-MC-8 ring of **1**.

contains all of the Mn^{III} ions and two of the Ho^{III} ions (Ho2 and Ho2a) (Figure 2). Two additional Ho^{III} ions (Ho1 and Ho1a) can be considered captured in the core of the MC. The standard metallacrown topology of M–N–O–M is retained in this ring for all bonds except the bridge between Mn3 (Mn3a) and Mn2 (Mn2a).

Each Ho^{III} ion is eight-coordinate. Ho1 is surrounded by eight oxygen atoms. Two of the oxygen atoms are carbonyl oxygen atoms from two acetate groups. A third carbonyl oxygen atom is derived from the carboxylate group of a sal²⁻ ligand. Three hydroximate oxygen atoms originate from three different shi³⁻ ligands: a μ_3 -oxygen and two μ_2 -oxygen atoms. The coordination sphere is completed by two μ_3 -hydroxide oxygen atoms. The average Ho1–O bond distance is 2.35 Å. Ho2 is also surrounded by eight oxygen atoms: one methanol oxygen atom, one carbonyl oxygen atom from an acetate anion, and three carbonyl oxygen atoms and three hydroximate oxygen atoms from three different shi³⁻ ligands. The hydroximate oxygen atoms consist of one μ_3 -oxygen and two μ_2 -oxygen atoms. Ho2 is surrounded by three five-membered chelate rings formed by the shi³⁻ ligands with the carbonyl and hydroximate oxygen atom pairs. The average Ho2–O bond distance is 2.33 Å. Each Mn^{III} ion is six-coordinate with an apparent Jahn–Teller axis. The equatorial plane of Mn1 contains two chelate rings from two shi³⁻ ligands. The first is a five-membered chelate ring formed by one carbonyl oxygen atom and a μ_2 -hydroximate oxygen atom. Trans to this ring is a six-membered ring formed by a phenolate oxygen atom and a hydroximate nitrogen atom. The axial positions are filled by a carbonyl oxygen atom from an acetate anion and a methanol oxygen

atom with a clear Jahn–Teller elongation (average Mn1–O_{JT} = 2.33 Å) that supports a 3+ oxidation state. The average Mn1–N/O bond distance is 2.05 Å. The equatorial plane of Mn2 consists of a μ_2 -hydroximate oxygen atom, a μ_3 -hydroxide oxygen atom, and a six-membered chelate ring formed by a phenolate oxygen atom and hydroximate nitrogen atom of a shi³⁻ ligand. The axial positions are occupied by a μ_2 -carbonyl oxygen atom from a sal²⁻ ligand and a μ_4 -hydroximate oxygen atom from a different shi³⁻ ligand. The Jahn–Teller elongation axis (average Mn2–O_{JT} = 2.29 Å) and the average Mn2–N/O bond distance of 2.06 Å confirm a 3+ oxidation state. Mn3 is surrounded by two six-membered chelate rings in the equatorial plane. The first is formed by a phenolate oxygen atom and a μ_2 -carbonyl oxygen atom from a sal²⁻ ligand, and the second chelate ring is formed by a phenolate oxygen atom and a hydroximate nitrogen atom from an shi³⁻ ligand. Two methanol oxygen atoms occupy the axial positions and form the Jahn–Teller axis (average Mn–O_{JT} = 2.31 Å). Again, the presence of a Jahn–Teller axis along with the average Mn3–N/O bond distance of 2.04 Å support a 3+ oxidation state assignment.

Numerous bridges exist between the metal centers (Figures 1 and 2). Ho1 is bridged to Ho1a via a μ_3 -oxide; to Ho2 via one acetate anion and two hydroximate oxygen atoms, a μ_3 -O and a μ_2 -O derived from hydroximates; to Mn1 via a μ_2 -O and the metallacrown N–O linkage; to Mn2 via two μ_3 -O hydroximate oxygens; to Mn2a via a carboxylate group of a sal²⁻ ligand and the MC N–O linkage; and to Mn1a via an acetate anion. Ho2 is connected to Mn1 via an N–O MC linkage, to Mn2 via a μ_2 -O hydroximate oxygen, and to Mn3 via another N–O MC linkage. Mn1 is bridged to Mn2a via an N–O MC linkage. A symmetry-related Mn2 is linked to Mn1a via an N–O MC bridge and to Mn3 via one MC N–O bridge and a μ_2 -O from a carbonyl oxygen. There is no direct connection between Mn1 and Mn2 or between Mn1 and Mn3.

Variable-temperature dc magnetic susceptibility measurements indicate that complexes **1** and **3** are dominated by antiferromagnetic exchange interactions at low temperatures (Figures S2 and S3). The χT product at 300 K (**1**, 66.7 cm³ K mol⁻¹; **3**, 69.1 cm³ K mol⁻¹), initially increases with decreasing temperature and then decreases to 39.3 and 45.5 cm³ K mol⁻¹, respectively, at 5 K. For **1** and **3** the room-temperature χT value is less than that expected for the four isolated Ln^{III} ions and six isolated Mn^{III} ions (~74 cm³ K mol⁻¹ for both **1** and **3**). Neither the spin nor the zero-field splitting of the ground state was able to be determined from variable-field dc magnetization measurements of **1** and **3** at 5 K. Additionally, the magnetization data do not saturate in fields as high as 5.5 T (Figures S4 and S5), indicating a high density of states within kT of the ground spin state.

Variable-temperature ac magnetic susceptibility measurements were performed on **1** (Figures S6 and S7) and **3** (Figures S8 and S9) in zero applied dc magnetic field with a 3.5 G ac alternating drive field operating at frequencies between 10 and 1000 Hz. The out-of-phase magnetic susceptibility increases below 5 K and the signal is frequency

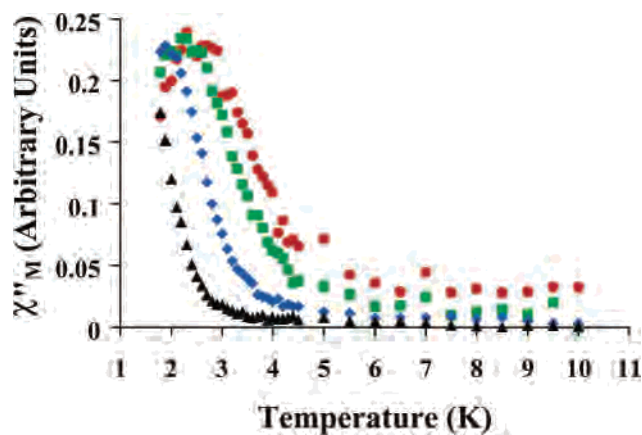


Figure 3. Variable-temperature out-of-phase ac magnetic susceptibility of **3** in DMF frozen solution. (●, 1000; ■, 500; ◆, 100; ▲, 10 Hz)

dependent—a characteristic of SMMs and spin glasses. The blocking temperatures for **1** and **3** could not be determined due to the 1.8 K temperature limitation of the Quantum Design MPMS SQUID magnetometer. In addition, from the very weak out-of-phase susceptibility values for **1**, the blocking temperature is expected to be well below 1.8 K. For **1** and **3** the in-phase magnetic susceptibility is also frequency dependent below 5 K, and extrapolation of the $\chi'T$ product before the divergence of χ' and χ'' yields a value of $31.4 \text{ cm}^3 \text{ K mol}^{-1}$ for **1** and $40.9 \text{ cm}^3 \text{ K mol}^{-1}$ for **3**.

To verify that the solid-state frequency-dependent behavior of **1** and **3** was a molecular phenomenon, (i.e., SMM behavior), frozen solutions of **1** and **3** in DMF were subjected to ac magnetic susceptibility experiments. The experiments reveal that **1** does not possess an out-of-phase signal above 1.8 K (Figures S10 and S11). Since complex **1** does not possess frequency-dependent behavior in solution, we attribute the solid-state behavior to either glassy behavior or the onset of magnetic ordering. We have examined the packing of the molecules in an effort to discern whether there are any obvious intermolecular interactions that could lead to an increase in magnetic relaxation in the solid state. There are no direct hydrogen bonds between the molecules; however, there is a hydrogen bond from an oxygen atom of an axial methanol of Mn1 to a water molecule in the lattice (2.57 Å). This water molecule is then hydrogen bonded to an oxygen atom of an axial methanol of Mn3 of a second Ho_4Mn_6 molecule (2.88 Å). The hydrogen bonds are perpetuated along the *a* axis. Furthermore, the molecules are tightly packed. Ho2 of one molecule is only 5.52 Å from a Ho2 of a second molecule along the *b* axis. In addition, along the *a* axis, Mn1 and Mn3 ions of separate molecules are about 7.83 Å apart. Thus, there are possibilities for both dipolar and hydrogen-bond pathways to mediate intermolecular exchange and facilitate short-range magnetic order or glassy behavior.

In contrast, complex **3** retains frequency-dependent ac susceptibility behavior, and a blocking temperature is observable above 2 K at 1000 Hz (Figures 3 and 4). We estimate that $U_{\text{eff}} = 11 \text{ cm}^{-1}$ and $\tau_0 = 2.6 \times 10^{-7} \text{ s}$, which

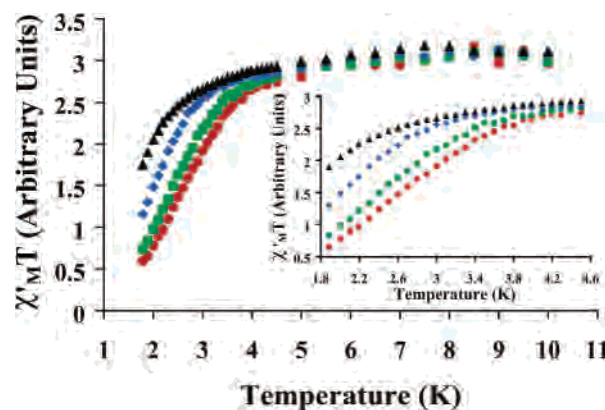


Figure 4. Variable-temperature in-phase ac magnetic susceptibility of **3** in DMF frozen solution. Inset: highlight of low-temperature data. (●, 1000; ■, 500; ◆, 100; ▲, 10 Hz)

leads to a relaxation time of 26 s at 1 K. The fact that the out-of-phase susceptibility possesses maxima above 1.8 K for frequencies higher than 100 Hz in solution but not in the solid state, coupled with a τ_0 value that is rather large, supports our claim that the slow relaxation time is due to possible SMM behavior. Moreover, the $\chi'T$ product between 10 and 6 K is almost constant for **3** in frozen DMF (Figure 4), while it decreases in the solid state; this supports the assertion that intermolecular interactions operating in the solid state have been eliminated in the frozen solution experiments, thus allowing the isolated molecular behavior to be revealed.

These data are remarkable in that they show that simple substitution of lanthanide cations in mixed $\text{Ln}^{\text{III}}\text{—TM}$ complexes dramatically affects the nature of the low-temperature magnetic behavior. Here it is observed that **3** ($\text{Dy}^{\text{III}}_4\text{Mn}^{\text{III}}_6$) exhibits behavior consistent with single-molecule magnetism, while **1** ($\text{Ho}^{\text{III}}_4\text{Mn}^{\text{III}}_6$) does not. The fact that **3** possesses slow relaxation of its magnetization was confirmed by critical frozen solution ac susceptibility studies. The solid-state ac data for **3** indicate that the low-frequency χ'' signal can be markedly reduced for some complexes, and this is likely a result of intermolecular interactions, which mask and complicate the analysis of the molecular magnetic behavior. Future studies will continue to examine the effects of Ln^{III} incorporation on the possible SMM behavior of large $\text{Ln}^{\text{III}}\text{—TM}$ complexes.

Acknowledgment. This work was supported by NSF CHE-0111428 to V.L.P. and NSF CHE-0616190 to M.L.K. We thank Reza Lolee of the Physics and Astronomy Department at Michigan State University and Meigan Aronson of the Department of Physics at the University of Michigan for use of their Quantum Design MPMS.

Supporting Information Available: Crystallographic data for **1** and **3**; magnetization plots and ac and dc magnetic susceptibility plots of **1** and **3**; χ''/χ' derivation. This material is available free of charge via the Internet at <http://pubs.acs.org>.

IC0621648